Available online at www.sciencedirect.com
ScienceDirect
Journal of Computational Physics 227 (2008) 4617–4629
JOURNAL OF COMPUTATIONAL PHYSICS
www.elsevier.com/locate/jcp

Modeling photonic crystals by boundary integral equations and Dirichlet-to-Neumann maps ☆

Jianhua Yuan [a], Ya Yan Lu [b,*], Xavier Antoine [c,d]

[a] Department of Mathematics, Beijing University of Posts and Telecommunications Beijing, China
[b] Department of Mathematics, City University of Hong Kong, Tat Chee Avenue, Kowloon, Hong Kong
[c] Institut Elie Cartan Nancy, Université Henri Poincaré Nancy 1, Vandoeuvre-lès-Nancy Cedex, France
[d] Département de Génie Industriel, Ecole Nationale Supérieure des Mines de Nancy, Nancy Cedex, France

Received 30 August 2007; received in revised form 24 December 2007; accepted 12 January 2008
Available online 26 January 2008

Abstract

Efficient numerical methods for analyzing photonic crystals (PhCs) can be developed using the Dirichlet-to-Neumann (DtN) maps of the unit cells. The DtN map is an operator that takes the wave field on the boundary of a unit cell to its normal derivative. In frequency domain calculations for band structures and transmission spectra of finite PhCs, the DtN maps allow us to reduce the computation to the boundaries of the unit cells. For two-dimensional (2D) PhCs with unit cells containing circular cylinders, the DtN maps can be constructed from analytic solutions (the cylindrical waves). In this paper, we develop a boundary integral equation method for computing DtN maps of general unit cells containing cylinders with arbitrary cross sections. The DtN map method is used to analyze band structures for 2D PhCs with elliptic and other cylinders.

Keywords: Photonic crystal; Numerical method; Boundary integral equation; Dirichlet-to-Neumann map; Band structures

1. Introduction

Photonic crystals (PhCs) [1–3] are periodic structures with a period on the scale of light wavelength. They have attracted much attention in recent years due to their unusual ability to control and manipulate light. Optical components and devices made of PhCs exhibit many unique functionalities, such as cavities with ultra-small mode volumes, ultra-compact waveguide bends, superprism effect, self-guiding, negative refractive index, slow light, etc. Efficient numerical methods are needed to analyze fundamental properties of PhCs and to design and optimize PhC components and devices.

☆ This research was partially supported by National Science Foundation of China (Project No. 10701016) and a grant from City University of Hong Kong (Project No. 7001943).
* Corresponding author.
E-mail address: mayylu@cityu.edu.hk (Y.Y. Lu).

0021-9991/$ - see front matter © 2008 Elsevier Inc. All rights reserved.
doi:10.1016/j.jcp.2008.01.014

The most important property of a PhC is its band structure of the spectrum. The band structure comprises dispersion relations between the frequency and the Bloch wave vector for waves allowed to propagate in the PhC. Many numerical methods have been developed for computing band structures. Time domain methods [5,6] have been used, but most existing techniques rely on frequency domain formulations. In the standard frequency domain formulation [3], the band structure problem is an eigenvalue problem on a unit cell of the PhC, where ω^2 (ω is the angular frequency) is the eigenvalue and the components of the Bloch wave vector are parameters. For a non-dispersive medium, the eigenvalue problem is linear, but it becomes nonlinear if the medium is dispersive [4]. A number of numerical methods using this formulation rely on expanding the eigenfunction in some series on the unit cell. The popular plane wave expansion method [7–11] uses the Fourier series, but other series can also be used [12,13]. Alternatively, the eigenvalue problem can be solved by a direct discretization of the unit cell. Numerical methods following this approach include the finite element method [14–16], the finite difference methods [17–20], the pseudospectral method [21], the cell method [22], the moving least squares method [23], the multiple multipole method [24], etc. For a non-dispersive medium, these methods give rise to eigenvalue problems of large matrices which are sparse in some cases. For dispersive media, the matrices depend on the frequency, the eigenvalue problem is nonlinear and more difficult to solve.

The band structure can also be calculated using alternative formulations where ω is regarded as a parameter and the eigenvalue is related to a component of the Bloch wave vector. In a formulation on the unit cell, this gives rise to a linear eigenvalue problem even when the medium is dispersive [25]. Furthermore, we can reformulate the eigenvalue problem to the boundary of the unit cell using the transfer matrix [26,27], the scattering matrix [28,34] or the Dirichlet-to-Neumann map [29,30] formalisms. These reformulations give rise to linear eigenvalue problems (even for dispersive media) for rather small matrices when they are discretized. Of course, additional work is needed to calculate the transfer matrix, the scattering matrix or the DtN map at each frequency. Although the transfer matrix is easy to calculate [26,27], the method suffers numerical instability. The scattering matrix can be constructed using a multipole method with lattice sums techniques [28] or other numerical methods for diffractive optics such as the Fourier modal method [31,32] and the finite element method [33,34]. The DtN map is an operator that maps the wave field on the boundary of the unit cell to its normal derivative. It can be approximated by a $J \times J$ matrix, if the wave field inside the unit cell is approximated by the linear combination of J special solutions. For two-dimensional (2D) PhCs where each unit cell contains exactly one circular cylinder, we have used the cylindrical waves as the special solutions [29,30]. In that case, the DtN map can be efficiently constructed using $O(J^3)$ operations. Based on the DtN map of the unit cell, the band structure can be calculated from standard matrix eigenvalue problems. Since the typical value of J is quite small, the DtN map method for band structure calculation is highly competitive. The DtN maps can also be used to derive efficient numerical methods for analyzing PhCs of finite size [35,36].

In this paper, we extend the DtN map method to 2D photonic crystals composed of identical and parallel cylinders with arbitrary cross sections. In Section 2, we first present improved eigenvalue formulations based on the DtN maps. Compared with the formulations used in [29], the new formulations are simpler and involve smaller matrices in some cases. In Section 3, we develop the boundary integral equation method for unit cells containing cylinders of arbitrary cross sections. In such a general unit cell, simple analytic solutions are not available. Our approach is to calculate the special solutions needed for constructing the DtN map by solving scattering problems of the cylinder with different plane incident waves. Since the size of the cylinder cross section is on the order of the wavelength, the integral equations formulated on the boundary of the cylinder require a relatively small number of discretization points. The different solutions corresponding to different incident waves can be efficiently solved together, as they are related to linear systems with an identical coefficient matrix and different right hand sides. We illustrate our method by band structure calculations for square and rectangular lattices.

2. Eigenvalue problems

For time harmonic electro-magnetic waves propagating in a 2D medium, the governing equation is

$$\rho \frac{\partial}{\partial x}\left(\frac{1}{\rho}\frac{\partial u}{\partial x}\right) + \rho \frac{\partial}{\partial y}\left(\frac{1}{\rho}\frac{\partial u}{\partial y}\right) + k_0^2 n^2 u = 0, \tag{1}$$

where $k_0 = \omega/c$ is the free space wavenumber, ω is the angular frequency, c is the speed of light in vacuum, $n = n(\mathbf{x})$ is the refractive index function and $\mathbf{x} = (x, y)$. For the E polarization, u is the z-component of the electric field and $\rho = 1$. For the H polarization, u is the z-component of the magnetic field and $\rho = n^2$. For a 2D PhC, the refractive index function is periodic in two distinct directions. We have two vectors $\mathbf{a}_1$ and $\mathbf{a}_2$, such that

$$n(\mathbf{x}) = n(\mathbf{x} + l_1\mathbf{a}_1 + l_2\mathbf{a}_2), \tag{2}$$

where l_1 and l_2 are arbitrary integers. As shown in Fig. 1(a), the parallelogram Ω specified by the vectors $\mathbf{a}_1$ and $\mathbf{a}_2$, i.e.,

$$\Omega = \{\mathbf{x} = s_1\mathbf{a}_1 + s_2\mathbf{a}_2 \mid 0 < s_1, s_2 < 1\} \tag{3}$$

is a unit cell of the PhC. Two edges of Ω are Γ_1 and Γ_2 given below

$$\Gamma_1 = \{\mathbf{x} = s_1\mathbf{a}_1 \mid 0 < s_1 < 1\}, \quad \Gamma_2 = \{\mathbf{x} = s_2\mathbf{a}_2 \mid 0 < s_2 < 1\}. \tag{4}$$

The other two edges of Ω are $\mathbf{a}_2 + \Gamma_1$ and $\mathbf{a}_1 + \Gamma_2$. We also let v_1 and v_2 be two unit vectors perpendicular to $\mathbf{a}_1$ and $\mathbf{a}_2$, respectively. These two vectors will serve as the unit normal vector of the boundary of Ω. We can choose v_1 and v_2 to be the inward unit normal vector of Ω on Γ_1 and Γ_2, then they are the outward normal vector on the other two edges of Ω.

For 2D PhCs, we consider Bloch wave solutions of the Helmholtz equation (1) given as

$$u(\mathbf{x}) = e^{i\mathbf{k}\cdot\mathbf{x}}\Psi(\mathbf{x}), \tag{5}$$

where $\mathbf{k} = (\alpha, \beta)$ is the Bloch wave vector and Ψ follows the same periodic condition (2) as the refractive index function. This implies that u satisfies the following quasi-periodic conditions:

$$u(\mathbf{x} + \mathbf{a}_1) = \rho_1 u(\mathbf{x}), \quad u(\mathbf{x} + \mathbf{a}_2) = \rho_2 u(\mathbf{x}), \tag{6}$$

where $\rho_1 = \exp(i\mathbf{k}\cdot\mathbf{a}_1)$ and $\rho_2 = \exp(i\mathbf{k}\cdot\mathbf{a}_2)$. Alternatively, we can write down the quasi-periodic conditions in terms of u and its normal derivatives on edges of Ω. The normal derivatives follow the unit normal vectors v_1 and v_2 chosen earlier. We have

$$u(\mathbf{x} + \mathbf{a}_2) = \rho_2 u(\mathbf{x}), \quad \frac{\partial u}{\partial v_1}(\mathbf{x} + \mathbf{a}_2) = \rho_2 \frac{\partial u}{\partial v_1}(\mathbf{x}), \quad \mathbf{x} \in \Gamma_1, \tag{7}$$

$$u(\mathbf{x} + \mathbf{a}_1) = \rho_1 u(\mathbf{x}), \quad \frac{\partial u}{\partial v_2}(\mathbf{x} + \mathbf{a}_1) = \rho_1 \frac{\partial u}{\partial v_2}(\mathbf{x}), \quad \mathbf{x} \in \Gamma_2. \tag{8}$$

In the standard formulation [3], Eq. (1) and boundary conditions (7) and (8) give rise to an eigenvalue problem on Ω, where α and β are given parameters and ω^2 (or k_0^2) is the eigenvalue. Most existing numerical methods use this formulation. The solutions give rise to a discrete sequence of dispersion relations

$$\omega = \omega_k(\mathbf{k}), \quad k = 1, 2, \ldots \tag{9}$$

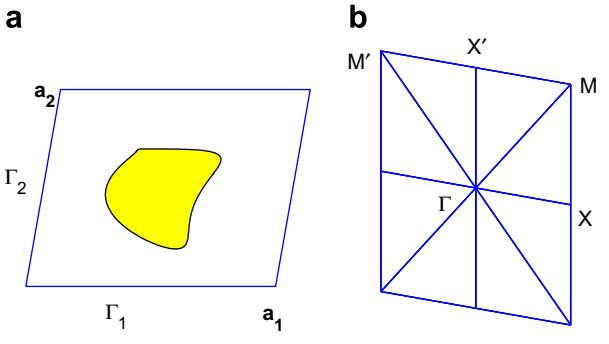

Fig. 1. (a) The unit cell Ω for a photonic crystal with two translation vectors $\mathbf{a}_1$ and $\mathbf{a}_2$. (b) The first Brillouin zone $\mathcal{B}$ with points Γ, X, M, X' and M' corresponding to $\pi\mathbf{b}_1$, $\pi(\mathbf{b}_1 + \mathbf{b}_2)$, $\pi\mathbf{b}_2$ and $\pi(\mathbf{b}_2 - \mathbf{b}_1)$, respectively.

For lossless media, the frequencies ω_k are real and they can be ordered as an increasing sequence. Each dispersion relationship is a surface of two variables α and β. If for some integer k, the maximum of ω_k is less than the minimum of ω_{k+1}, we have a band gap:

$$(\max_{\mathbf{k}} \omega_k(\mathbf{k}), \min_{\mathbf{k}} \omega_{k+1}(\mathbf{k})).$$

If the frequency ω is in a band gap, propagating Bloch waves do not exist for any real α and β, therefore, waves at this frequency cannot propagate in the PhC.

Due to the periodicity of the PhC, ω_k is a periodic function of the Bloch wave vector $\mathbf{k}$ satisfying

$$\omega_k(\mathbf{k} + 2\pi l_1 \mathbf{b}_1 + 2\pi l_2 \mathbf{b}_2) = \omega_k(\mathbf{k}), \tag{10}$$

where l_1 and l_2 are arbitrary integers, $\mathbf{b}_1$ and $\mathbf{b}_2$ are vectors satisfying

$$\mathbf{b}_j \cdot \mathbf{a}_k = \delta_{jk} = \begin{cases} 1 & \text{if } j = k, \\ 0 & \text{if } j \neq k. \end{cases} \tag{11}$$

Therefore, it is only necessary to calculate the dispersion relations (9) on the first Brillouin zone

$$\mathcal{B} = \{\mathbf{k} = s_1 \mathbf{b}_1 + s_2 \mathbf{b}_2 \mid -\pi < s_1, s_2 < \pi\}. \tag{12}$$

For the unit cell shown in Fig. 1(a), the corresponding first Brillouin zone $\mathcal{B}$ is depicted in Fig. 1(b). The points Γ, X, M, X' and M' correspond to $\pi\mathbf{b}_1$, $\pi(\mathbf{b}_1 + \mathbf{b}_2)$, $\pi\mathbf{b}_2$ and $\pi(\mathbf{b}_2 - \mathbf{b}_1)$, respectively. For a lossless medium where the refractive index is real, if u is a solution of the Helmholtz equation (1), then $\bar{u}$ (the complex conjugate of u) is also a solution. If u is a Bloch wave solution with a wave vector $\mathbf{k}$, then $\overline{u}$ is a Bloch wave solution with wave vector $-\mathbf{k}$. This implies that the dispersion relations are even functions of $\mathbf{k}$, i.e.,

$$\omega_k(\mathbf{k}) = \omega_k(-\mathbf{k}). \tag{13}$$

Therefore, if $n(\mathbf{x})$ is real, we only need to compute the dispersion relations on one half of the first Brillouin zone. Furthermore, using (13) and the periodicity (10), we can deduce that the dispersion relations are symmetric with respect to the mid-point on each edge of the first Brillouin zone. For example, on the top edge given by

$$\mathbf{k} = \pi\mathbf{b}_2 + \pi s_1 \mathbf{b}_1, \quad -1 < s_1 < 1,$$

we have

$$\omega_k(\pi\mathbf{b}_2 + \pi s_1 \mathbf{b}_1) = \omega_k(-\pi\mathbf{b}_2 - \pi s_1 \mathbf{b}_1) = \omega_k(\pi\mathbf{b}_2 - \pi s_1 \mathbf{b}_1). \tag{14}$$

Using other symmetries, it is often possible to further reduce the computation domain of $\mathbf{k}$. In practice, the dispersion relations are often calculated on edges of the irreducible Brillouin zone. If the medium is dispersive (thus, the refractive index n depends on ω), this eigenvalue problem is nonlinear and more difficult to solve.

Alternatively, we can consider ω as a given parameter and formulate the band structure problem as eigenvalue problems with an eigenvalue related to the Bloch wave vector $\mathbf{k}$. Let us expand $\mathbf{k}$ as $\mathbf{k} = \gamma_1 \mathbf{b}_1 + \gamma_2 \mathbf{b}_2$. If γ_1 is assumed to be a given parameter, we can formulate an eigenvalue problem for γ_2. Notice that $\gamma_1 = \mathbf{k} \cdot \mathbf{a}_1$ and $\gamma_2 = \mathbf{k} \cdot \mathbf{a}_2$. To remove the eigenvalue γ_2 from the boundary condition (7), we re-write the Bloch wave given in (5) as

$$u(\mathbf{x}) = \mathrm{e}^{\mathrm{i}\gamma_2 \mathbf{b}_2 \cdot \mathbf{x}} \phi(\mathbf{x}). \tag{15}$$

From (1), we obtain the following equation for ϕ:

$$\rho \nabla \cdot \left(\frac{1}{\rho} \nabla \phi\right) + k_0^2 n^2 \phi + \mathrm{i}\gamma_2 \mathbf{b}_2 \cdot \left[\nabla \phi + \rho \nabla \cdot \left(\frac{1}{\rho} \phi\right)\right] - \gamma_2^2 \|\mathbf{b}_2\|^2 \phi = 0. \tag{16}$$

From the quasi-periodic conditions of u, it is easy to see that ϕ is quasi-periodic in $\mathbf{a}_1$ direction and periodic in $\mathbf{a}_2$ direction. That is

$$\phi(\mathbf{x} + \mathbf{a}_1) = \rho_1 \phi(\mathbf{x}), \quad \phi(\mathbf{x} + \mathbf{a}_2) = \phi(\mathbf{x}). \tag{17}$$

This gives rise to the boundary conditions of ϕ:

$$\phi(\mathbf{x}+\mathbf{a}_2)=\phi(\mathbf{x}),\quad \frac{\partial\phi}{\partial v_1}(\mathbf{x}+\mathbf{a}_2)=\frac{\partial\phi}{\partial v_1}(\mathbf{x}),\quad \mathbf{x}\in\Gamma_1, \tag{18}$$

$$\phi(\mathbf{x}+\mathbf{a}_1)=\rho_1\phi(\mathbf{x}),\quad \frac{\partial\phi}{\partial v_2}(\mathbf{x}+\mathbf{a}_1)=\rho_1\frac{\partial\phi}{\partial v_2}(\mathbf{x}),\quad \mathbf{x}\in\Gamma_2. \tag{19}$$

Therefore, we obtain a quadratic eigenvalue problem (16), (18) and (19) for eigenfunction ϕ and eigenvalue γ_2. Notice that the quadratic eigenvalue problem can be turned into a linear eigenvalue problem if we change (16) into a system of two equations with an additional function $\varphi=\gamma_2\phi$. This eigenvalue problem is still formulated on the unit cell Ω and it is linear even if the medium is dispersive.

The band structure eigenvalue problem can be further reduced to the edges of the unit cell Ω. The transfer matrix approach [26,27] is easy to implement, but it suffers from numerical instabilities. The scattering matrix approach [28,34] relies on decomposing the wave field as the sum of its forward and backward components, i.e, $u=u^+ + u^-$, around the edges Γ_1 and $\Gamma_1+\mathbf{a}_2$. If we denote $u^\pm$ on Γ_1 and $\Gamma_1+\mathbf{a}_2$ as $u_0^\pm$ and $u_1^\pm$, respectively, then the scatter matrix $\mathcal{S}$ satisfies

$$\mathcal{S}\begin{bmatrix}u_0^+\\ u_1^-\end{bmatrix}=\begin{bmatrix}\mathcal{S}_{11} & \mathcal{S}_{12}\\ \mathcal{S}_{21} & \mathcal{S}_{22}\end{bmatrix}\begin{bmatrix}u_0^+\\ u_1^-\end{bmatrix}=\begin{bmatrix}u_0^-\\ u_1^+\end{bmatrix}. \tag{20}$$

Here, $\mathcal{S}$ is given as a 2×2 matrix where each entry is an operator acting on functions defined on edges of Ω. The quasi-periodicity in $\mathbf{a}_2$ direction implies

$$u_1^+=\rho_2 u_0^+,\quad u_1^-=\rho_2 u_0^-. \tag{21}$$

This leads to the following eigenvalue problem

$$\begin{bmatrix}\mathcal{S}_{11} & -I\\ \mathcal{S}_{21} & 0\end{bmatrix}\begin{bmatrix}u_0^+\\ u_0^-\end{bmatrix}=\rho_2\begin{bmatrix}0 & -\mathcal{S}_{12}\\ I & -\mathcal{S}_{22}\end{bmatrix}\begin{bmatrix}u_0^+\\ u_0^-\end{bmatrix}, \tag{22}$$

where I is the identity operator and ρ_2 is the eigenvalue. Notice that this is a linear eigenvalue problem even if the medium is dispersive. The scattering matrix $\mathcal{S}$ can be calculated by analyzing one layer of the PhC, i.e., $\mathbf{x}=s_1\mathbf{a}_1+s_2\mathbf{a}_2$ for $-\infty<s_1<\infty$ and $0<s_2<1$, as a diffraction grating problem. Existing numerical methods for diffraction gratings, such as the Fourier modal method [31,32], the finite element method [33,34] and the multipole method [28], can be used to find $\mathcal{S}$.

Another reformulation of the band structure eigenvalue problem is based on the Dirichlet-to-Neumann maps. In [29,30], we formulated the eigenvalue problems for square and triangular lattices, respectively. In the following, we derive improved formulations for general lattice structures. These new formulations are simpler and they involve smaller matrices in some cases. If we denote $\{u,\partial_{v_1}u\}$ on the edges Γ_1 and $\Gamma_1+\mathbf{a}_2$ by $\{u_0,\partial_{v_1}u_0\}$ and $\{u_1,\partial_{v_1}u_1\}$, respectively, the reduced DtN map $\mathcal{M}$ gives

$$\mathcal{M}\begin{bmatrix}u_0\\ u_1\end{bmatrix}=\begin{bmatrix}\mathcal{M}_{11} & \mathcal{M}_{12}\\ \mathcal{M}_{21} & \mathcal{M}_{22}\end{bmatrix}\begin{bmatrix}u_0\\ u_1\end{bmatrix}=\begin{bmatrix}\partial_{v_1}u_0\\ \partial_{v_1}u_1\end{bmatrix}. \tag{23}$$

Similar to the scatter matrix $\mathcal{S}$, the reduced DtN map $\mathcal{M}$ is a 2×2 matrix with operator entries. Using the quasi-periodic condition in $\mathbf{a}_2$ direction, i.e.,

$$u_1=\rho_2 u_0,\quad \partial_{v_1}u_1=\rho_2\partial_{v_1}u_0,$$

we obtain the following linear eigenvalue problem

$$\begin{bmatrix}\mathcal{M}_{11} & -I\\ \mathcal{M}_{21} & 0\end{bmatrix}\begin{bmatrix}u_0\\ \partial_{v_1}u_0\end{bmatrix}=\rho_2\begin{bmatrix}-\mathcal{M}_{12} & 0\\ -\mathcal{M}_{22} & I\end{bmatrix}\begin{bmatrix}u_0\\ \partial_{v_1}u_0\end{bmatrix}, \tag{24}$$

where ρ_2 is the eigenvalue. It turns out that the reduced DtN map $\mathcal{M}$ can be easily calculated from the DtN map Λ of the unit cell Ω satisfying

$$\Lambda\begin{bmatrix}u_0\\ v_0\\ u_1\\ v_1\end{bmatrix}=\begin{bmatrix}\Lambda_{11} & \Lambda_{12} & \Lambda_{13} & \Lambda_{14}\\ \Lambda_{21} & \Lambda_{22} & \Lambda_{23} & \Lambda_{24}\\ \Lambda_{31} & \Lambda_{32} & \Lambda_{33} & \Lambda_{34}\\ \Lambda_{41} & \Lambda_{42} & \Lambda_{43} & \Lambda_{44}\end{bmatrix}\begin{bmatrix}u_0\\ v_0\\ u_1\\ v_1\end{bmatrix}=\begin{bmatrix}\partial_{v_1}u_0\\ \partial_{v_2}v_0\\ \partial_{v_1}u_1\\ \partial_{v_2}v_1\end{bmatrix}, \tag{25}$$

where v_0 and v_1 denote u on the edges Γ_2 and $\Gamma_2 + \mathbf{a}_1$, respectively, and $\partial_{\nu_2} v_0$ and $\partial_{\nu_2} v_1$ denote the normal derivatives of u there. Using the quasi-periodic conditions in $\mathbf{a}_1$ direction, i.e., $v_1 = \rho_1 v_0$ and $\partial_{\nu_2} v_1 = \rho_1 \partial_{\nu_2} v_0$, and the second and fourth equations of (25), we can eliminate $\partial_{\nu_2} v_0$ and obtain an equation for v_0:

$$Dv_0 = (\Lambda_{41} - \rho_1 \Lambda_{21}) u_0 + (\Lambda_{43} - \rho_1 \Lambda_{23}) u_1, \tag{26}$$

where

$$D = \rho_1^2 \Lambda_{24} + \rho_1 (\Lambda_{22} - \Lambda_{44}) - \Lambda_{42}.$$

The above gives rise to $v_0 = K_1 u_0 + K_2 u_1$, where

$$K_1 = D^{-1}(\Lambda_{41} - \rho_1 \Lambda_{21}), \quad K_2 = D^{-1}(\Lambda_{43} - \rho_1 \Lambda_{23}).$$

We can insert these results into the first and third equations of (25) and obtain

$$\mathcal{M} = \begin{bmatrix} \Lambda_{11} & \Lambda_{13} \\ \Lambda_{31} & \Lambda_{33} \end{bmatrix} + \begin{bmatrix} \Lambda_{12} + \rho_1 \Lambda_{14} \\ \Lambda_{32} + \rho_1 \Lambda_{34} \end{bmatrix} [K_1, K_2]. \tag{27}$$

In the three eigenvalue formulations (16), (18), (19), (22) and (24), we have assumed that the frequency ω and a component of the Bloch wave vector $\gamma_1 = \mathbf{k} \cdot \mathbf{a}_1$ are given parameters. The eigenvalue is either $\gamma_2 = \mathbf{k} \cdot \mathbf{a}_2$ or $\rho_2 = e^{i\gamma_2}$. Similarly, we can derive band structure eigenvalue formulations where ω and γ_2 are given parameters and γ_1 or $\rho_1 = e^{i\gamma_1}$ is the eigenvalue. For the DtN map formulation, applying the quasi-periodic conditions in $\mathbf{a}_2$ direction to (25), we can find another reduced DtN map $\mathcal{N}$ satisfying

$$\mathcal{N} \begin{bmatrix} v_0 \\ v_1 \end{bmatrix} = \begin{bmatrix} \mathcal{N}_{11} & \mathcal{N}_{12} \\ \mathcal{N}_{21} & \mathcal{N}_{22} \end{bmatrix} \begin{bmatrix} v_0 \\ v_1 \end{bmatrix} = \begin{bmatrix} \partial_{\nu_2} v_0 \\ \partial_{\nu_2} v_1 \end{bmatrix}. \tag{28}$$

Then, the quasi-periodic condition in $\mathbf{a}_1$ direction gives rise to the following eigenvalue problem:

$$\begin{bmatrix} \mathcal{N}_{11} & -I \\ \mathcal{N}_{21} & 0 \end{bmatrix} \begin{bmatrix} v_0 \\ \partial_{\nu_2} v_0 \end{bmatrix} = \rho_1 \begin{bmatrix} -\mathcal{N}_{12} & 0 \\ -\mathcal{N}_{22} & I \end{bmatrix} \begin{bmatrix} v_0 \\ \partial_{\nu_2} v_0 \end{bmatrix}. \tag{29}$$

In principle, the dispersion relations in (9) are needed for all $\mathbf{k}$ in the irreducible Brillouin zone. If only the edges of the irreducible Brillouin zone are used, band gaps can be over estimated [40]. Our method can be used to compute the dispersion relations on the entire Brillouin zone. If the DtN eigenvalue formulation (24) is used, we need to vary two parameters ω and γ_1, and solve (24) for each selection of the parameters. Only eigenvalues on the unit circle, i.e. $|\rho_2| = 1$, are needed, since we are looking for Bloch waves with a real Bloch wave vector. In practice, the dispersion relations are often calculated on a few edges of the irreducible Brillouin zone. The two formulations (24) and (29) allow us to calculate the dispersion relations along lines parallel to $\mathbf{b}_2$ and $\mathbf{b}_1$, respectively. Next, we formulate eigenvalue problems on the two diagonals of the first Brillouin zone. On the diagonal given by $\mathbf{k} = s(\mathbf{b}_1 + \mathbf{b}_2)$ for $-\pi < s < \pi$, we have $\gamma_1 = \mathbf{k} \cdot \mathbf{a}_1 = \mathbf{k} \cdot \mathbf{a}_2 = \gamma_2$ and $\rho_1 = \rho_2$. Using the quasi-periodic conditions in both $\mathbf{a}_1$ and $\mathbf{a}_2$ directions, we can eliminate u_1, v_1, $\partial_{\nu_1} u_1$ and $\partial_{\nu_2} v_1$ in (25), and obtain the following eigenvalue problem:

$$\begin{bmatrix} \Lambda_{11} & \Lambda_{12} & -I & 0 \\ \Lambda_{21} & \Lambda_{22} & 0 & -I \\ \Lambda_{31} & \Lambda_{32} & 0 & 0 \\ \Lambda_{41} & \Lambda_{42} & 0 & 0 \end{bmatrix} U = \rho \begin{bmatrix} -\Lambda_{13} & -\Lambda_{14} & 0 & 0 \\ -\Lambda_{23} & -\Lambda_{24} & 0 & 0 \\ -\Lambda_{33} & -\Lambda_{34} & I & 0 \\ -\Lambda_{43} & -\Lambda_{44} & 0 & I \end{bmatrix} U, \tag{30}$$

where $U = [u_0; v_0; \partial_{\nu_1} u_0; \partial_{\nu_2} v_0]$ is a column vector given in the MATLAB notation ($u_0, v_0, \ldots$, are column vectors), and the eigenvalue is $\rho = \rho_1 = \rho_2$. On the other diagonal given by $\alpha = s(\mathbf{b}_2 - \mathbf{b}_1)$ for $-\pi < s < \pi$. We have $\gamma_2 = -\gamma_1$ and $\rho_2 = \rho_1^{-1}$. Eliminating u_1, v_0, $\partial_{\nu_1} u_1$ and $\partial_{\nu_2} v_0$ in (25), we have

$$\begin{bmatrix} \Lambda_{11} & \Lambda_{14} & -I & 0 \\ \Lambda_{41} & \Lambda_{44} & 0 & -I \\ \Lambda_{31} & \Lambda_{34} & 0 & 0 \\ \Lambda_{21} & \Lambda_{24} & 0 & 0 \end{bmatrix} U = \rho \begin{bmatrix} -\Lambda_{13} & -\Lambda_{12} & 0 & 0 \\ -\Lambda_{43} & -\Lambda_{42} & 0 & 0 \\ -\Lambda_{33} & -\Lambda_{32} & I & 0 \\ -\Lambda_{23} & -\Lambda_{22} & 0 & I \end{bmatrix} U, \tag{31}$$

where $U = [u_0; v_1; \partial_{\nu_1} u_0; \partial_{\nu_2} v_1]$ and the eigenvalue is $\rho = \rho_2 = \rho_1^{-1}$.

If N_1 and N_2 sampling points are used on Γ_1 and Γ_2 (and their opposite edges) of the unit cell Ω, respectively, the DtN map Λ is approximated by a $J \times J$ matrix, where $J = 2(N_1 + N_2)$. The operators $\mathcal{M}_{jk}$ for $j, k = 1, 2$, become $N_1 \times N_1$ matrices. The eigenvalue problems (24) and (29) involve $(2N_1) \times (2N_1)$ and $(2N_2) \times (2N_2)$ matrices, respectively. On the other hand, the eigenvalue problems on the diagonals, i.e., (30) and (31), involve $J \times J$ matrices. All these eigenvalue problems can be solved in $O(J^3)$ operations. Since the typical value of J is quite small, our method is highly competitive. Compared with our previous DtN formulations developed in [29], the new formulations (24) and (29)–(31) are simpler and they give smaller matrices along lines parallel to $\mathbf{b}_1$ or $\mathbf{b}_2$. For a triangular lattice, although the general treatment developed in this section is applicable, the approach based on hexagon unit cells developed in [30] is still preferred because of the symmetry.

3. DtN map by boundary integral equations

To find a matrix approximation to the DtN map Λ, we choose J sampling points on the boundary of unit cell Ω and approximate the general solution in Ω by a linear combination of J special solutions:

$$u(\mathbf{x}) = \sum_{j=1}^{J} c_j \phi_j(\mathbf{x}), \tag{32}$$

where ϕ_j satisfies the Helmholtz equation (1). Let the J sampling points on the boundary of Ω be $\mathbf{x}_1, \mathbf{x}_2, \ldots, \mathbf{x}_J$. If we use (32) to evaluate u at the sampling points, we obtain a $J \times J$ matrix Λ_1 that maps the coefficients $\{c_j\}$ to the J values of u on the boundary of Ω. In fact, the (k, j) entry of the matrix Λ_1 is $\phi_j(\mathbf{x}_k)$. We can also find the x and y derivatives of ϕ_j and evaluate the normal derivative of u at the J sampling points. This gives rise to another $J \times J$ matrix Λ_2 that maps $\{c_j\}$ to the normal derivatives of u at the J points. The (k, j) entry of the matrix Λ_2 is $\partial_\nu \phi_j(\mathbf{x}_k)$, where ν is a unit vector of the boundary at point $\mathbf{x}_k$. Then, the DtN map of the unit cell is approximated by the matrix $\Lambda = \Lambda_2 \Lambda_1^{-1}$.

If the unit cell contains a circular cylinder, we choose ϕ_j as cylindrical waves which are given analytically. At least for square and hexagon unit cells, the cylindrical waves give rise to accurate approximations of the DtN map Λ. Numerical experiments in [29,30] indicate an exponential convergence with respect to the number of points used on each edge of the unit cell. In the following, we consider a more general unit cell containing a cylinder of arbitrary cross section. Our approach is to let

$$\phi_j = \phi_j^{(i)} + \phi_j^{(s)},$$

where $\phi_j^{(i)}$ is a plane wave propagating with an incident angle τ_j and $\phi_j^{(s)}$ is the associated scattered wave. The incident angles are either $\tau_j = 2\pi j/J$ or $\tau_j = 2\pi(j - 0.5)/J$ depending on how the sampling points are chosen. We solve the scattered wave $\phi_j^{(s)}$ by a boundary integral equation method. The J different scattered waves correspond to the same scatterer and they can be efficiently solved together.

Let Ω_1 be the cross section of the cylinder in the unit cell, let n_1 and n_2 be the refractive indices of the cylinder and the surrounding medium, respectively, the scattering problem is formulated in the entire xy-plane $\mathbb{R}^2$ for a single cylinder. Let $\Omega_2 = \mathbb{R}^2 \setminus \overline{\Omega}_1$ be the domain outside the cylinder, the incident wave is given in Ω_2 as

$$\phi_j^{(i)}(\mathbf{x}) = \exp[\mathrm{i}k_0 n_2(x \cos \tau_j + y \sin \tau_j)],$$

and the scattered wave $\phi_j^{(s)}$ satisfies the Sommerfeld radiation condition at infinity. In our boundary integral formulation, we solve for two functions ψ and φ defined on the boundary Σ of domain Ω_1. Let $\nu(\mathbf{p})$ be the outward unit normal vector of Σ at a point $\mathbf{p}$, we have

$$\psi(\mathbf{p}) = \phi_j(\mathbf{p}), \quad \varphi(\mathbf{p}) = \frac{\partial \phi_j(\mathbf{p})}{\partial \nu(\mathbf{p})}.$$

For the H polarization, the normal derivative of ϕ_j is not continuous on Σ, then φ is defined as the limit from the outside of the cylinder, i.e., from Ω_2. Let G_l (for $l = 1, 2$) be the fundamental solution of the Helmholtz equation in the medium with refractive index n_l, i.e.,

$$G_l(\mathbf{p},\mathbf{q}) = \frac{\mathrm{i}}{4}H_0^{(1)}(k_0 n_l|\mathbf{p}-\mathbf{q}|),$$

we define the single- and double-layer integral operators by

$$(\mathcal{S}_l\mu)(\mathbf{p}) = 2\int_\Sigma G_l(\mathbf{p},\mathbf{q})\mu(\mathbf{q})\mathrm{d}s(\mathbf{q}), \quad \mathbf{p}\in\Sigma;$$
$$(\mathcal{K}_l\mu)(\mathbf{p}) = 2\int_\Sigma \frac{\partial G_l(\mathbf{p},\mathbf{q})}{\partial \nu(\mathbf{q})}\mu(\mathbf{q})\mathrm{d}s(\mathbf{q}), \quad \mathbf{p}\in\Sigma,$$

where μ is an arbitrary function defined on Σ. Then, ψ and φ satisfy the following integral equations:

$$(1+\mathcal{K}_1)\psi - \mathcal{S}_1\varphi = 0, \tag{33}$$

$$(1-\mathcal{K}_2)\psi + \gamma\mathcal{S}_2\varphi = (1-\mathcal{K}_2)\phi_j^{(i)} + \mathcal{S}_2\frac{\partial\phi_j^{(i)}}{\partial\nu}, \tag{34}$$

where $\gamma = 1$ and $\gamma = n_1^2/n_2^2$ for the E and H polarization, respectively. Once ψ and φ are solved, we can evaluate the total wave field at a point $\mathbf{p}$ in Ω_2 by

$$\phi_j(\mathbf{p}) = \phi_j^{(i)}(\mathbf{p}) + \int_\Sigma \frac{\partial G_2(\mathbf{p},\mathbf{q})}{\partial\nu(\mathbf{q})}\tilde{\psi}(\mathbf{q})\mathrm{d}s(\mathbf{q}) - \int_\Sigma G_2(\mathbf{p},\mathbf{q})\tilde{\varphi}(\mathbf{q})\mathrm{d}s(\mathbf{q}), \tag{35}$$

where

$$\tilde{\psi}(\mathbf{q}) = \psi(\mathbf{q}) - \phi_j^{(i)}(\mathbf{q}), \quad \tilde{\varphi}(\mathbf{q}) = \varphi(\mathbf{q}) - \frac{\partial\phi_j^{(i)}(\mathbf{q})}{\partial\nu(\mathbf{q})}, \quad \mathbf{q}\in\Sigma.$$

If we have a unit vector $\nu(\mathbf{p})$ at a point $\mathbf{p}\in\Omega_2$, we can evaluate the directional derivative at $\mathbf{p}$ by taking the derivative from (35) directly. That is

$$\frac{\partial\phi_j(\mathbf{p})}{\partial\nu(\mathbf{p})} = \frac{\partial\phi_j^{(i)}(\mathbf{p})}{\partial\nu(\mathbf{p})} + \int_\Sigma \frac{\partial^2 G_2(\mathbf{p},\mathbf{q})}{\partial\nu(\mathbf{p})\partial\nu(\mathbf{q})}\tilde{\psi}(\mathbf{q})\mathrm{d}s(\mathbf{q}) - \int_\Sigma \frac{\partial G_2(\mathbf{p},\mathbf{q})}{\partial\nu(\mathbf{p})}\tilde{\varphi}(\mathbf{q})\mathrm{d}s(\mathbf{q}). \tag{36}$$

To solve the integral Eqs. (33) and (34), we use a numerical method described in [37]. The method is especially suitable when the interface Σ is smooth. Starting from a parametric representation of Σ given by

$$\mathbf{q} = (x,y) = (\xi(\theta),\eta(\theta)), \quad 0\leqslant\theta\leqslant 2\pi,$$

we approximate φ and ψ by vectors of length m following a discretization of θ as $\theta_l = 2\pi l/m$ for $0\leqslant l<m$. The integral operators are approximated by $m\times m$ matrices through the following three steps. First, we transform the integral operators on Σ to those on $[0,2\pi]$. We have functions S_1, S_2, K_1 and K_2 satisfying

$$(\mathcal{S}_l\mu)(\vartheta) = \int_0^{2\pi} S_l(\vartheta,\theta)\mu(\theta)\mathrm{d}\theta, \quad (\mathcal{K}_l\mu)(\vartheta) = \int_0^{2\pi} K_l(\vartheta,\theta)\mu(\theta)\mathrm{d}\theta$$

for $l = 1, 2$, where

$$S_l(\vartheta,\theta) = \frac{\mathrm{i}\sigma}{2}H_0^{(1)}(k_0 n_l r), \quad K_l(\vartheta,\theta) = -\frac{\mathrm{i}k_0 n_l\rho}{2r}H_1^{(1)}(k_0 n_l r)$$

and

$$\mathbf{p} = (\xi(\vartheta),\eta(\vartheta)),$$
$$\mathbf{n} = (\eta'(\theta),-\xi'(\theta)),$$
$$\sigma = \sigma(\theta) = |\mathbf{q}'| = \sqrt{[\xi'(\theta)]^2 + [\eta'(\theta)]^2},$$
$$r = r(\vartheta,\theta) = |\mathbf{p}-\mathbf{q}| = \sqrt{[\xi(\vartheta)-\xi(\theta)]^2 + [\eta(\vartheta)-\eta(\theta)]^2},$$
$$\rho = \rho(\vartheta,\theta) = \mathbf{n}\cdot(\mathbf{q}-\mathbf{p}) = \eta'(\theta)[\xi(\theta)-\xi(\vartheta)] - \xi'(\theta)[\eta(\theta)-\eta(\vartheta)].$$

Next, we separate the logarithmic singularity in the integral operator kernels. For S_l and K_l, we have smooth functions $S_{l,1}$, $S_{l,2}$, $K_{l,1}$ and $K_{l,2}$ such that

$$S_l(\vartheta,\theta) = S_{l,1}(\vartheta,\theta)\ln\left(4\sin^2\frac{\vartheta-\theta}{2}\right) + S_{l,2}(\vartheta,\theta), \tag{37}$$

$$K_l(\vartheta,\theta) = K_{l,1}(\vartheta,\theta)\ln\left(4\sin^2\frac{\vartheta-\theta}{2}\right) + K_{l,2}(\vartheta,\theta), \tag{38}$$

where

$$S_{l,1} = -\frac{\sigma}{2\pi}J_0(k_0 n_l r), \quad K_{l,1} = \frac{k_0 n_l \rho}{2\pi r}J_1(k_0 n_l r),$$

$S_{l,2}$ and $K_{l,2}$ are evaluated using (37) and (38), except when $\vartheta = \theta$. In that case,

$$S_{l,2}(\theta,\theta) = \left[\frac{\mathrm{i}}{2} - \frac{C}{\pi} - \frac{1}{\pi}\ln\left(\frac{k_0 n_l \sigma}{2}\right)\right]\sigma,$$

$$K_{l,2}(\theta,\theta) = \frac{\eta'(\theta)\xi''(\theta) - \xi'(\theta)\eta''(\theta)}{2\pi\sigma^2},$$

where $C = 0.57721\ldots$ is the Euler's constant. Finally, we discretize the integral operators by quadrature formulas. For smooth functions, the standard trapezoidal rule is used. For the product of the logarithmic singularity with a smooth function, the following special quadrature formula is used. Assume that m is an even integer, we have

$$\int_0^{2\pi} \ln\left(4\sin^2\frac{\vartheta-\theta}{2}\right) f(\theta)\mathrm{d}\theta \approx \sum_{j=0}^{m-1} R_j(\vartheta) f(\theta_j),$$

where

$$R_j(\vartheta) = -\frac{4\pi}{m}\sum_{k=1}^{m/2-1}\frac{1}{k}\cos[k(\vartheta-\theta_j)] - \frac{4\pi}{m^2}\cos[m(\vartheta-\theta_j)/2].$$

More details can be found in [37]. With the integral operators approximated by matrices, the right hand side of (34) can be easily evaluated, φ and ψ can then be solved in $\mathrm{O}(m^3)$ operations. Afterward, for each sampling point $\mathbf{p}$ on the boundary of the unit cell Ω, we evaluate $\phi_j(\mathbf{p})$ and its normal derivative using (35) and (36). In that case, $\mathbf{p}$ is not on the interface Σ, the integral operators in (35) and (36) have smooth kernels, thus they can be easily discretized with the trapezoidal rule.

To construct the DtN map Λ, we need J special solutions corresponding to J different plane incident waves. We emphasize that the total required number of operations is still $\mathrm{O}(m^3)$, assuming that J is on the same order as m. This corresponds to solving J linear systems with the same coefficient matrix. The matrix approximations to the integral operators and the LU decomposition of the coefficient matrix are calculated only once.

4. Numerical examples

We first test our method for PhCs with square unit cells containing circular cylinders. For the examples in [29], we have obtained nearly identical results. For a circular cylinder, the scattering field $\phi_j^{(s)}$ associated with a plane incident wave $\phi_j^{(i)}$ can be solved analytically. This allows us to test our boundary integral equation method for solving $\phi_j^{(s)}$. The DtN-map method developed in [29] uses different special solutions (the cylindrical waves) to construct the DtN maps of the unit cells and also uses different eigenvalue formulations.

In this following, we illustrate our method by a few examples involving non-circular cylinders. First, we consider a rectangular lattice of elliptic air-holes in a background medium with dielectric constant $\epsilon_2 = n_2^2 = 11.4$. A unit cell is shown in Fig. 2(a). The periods in the x and y directions are L_1 and L_2, respectively. As in [38], we assume that $L_1 = 0.77L_2$. The minor and major axes of the elliptic air-holes are parallel to the x and y axes, respectively. The lengths of the semi-axes are $r_1 = 0.3L_2$ and $r_2 = 0.4L_2$. The PhC has reflec-

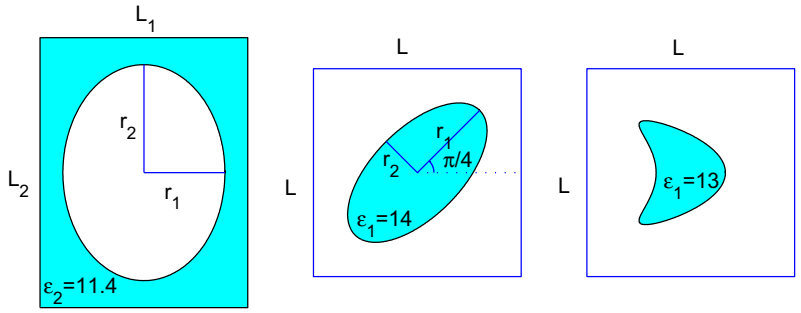

Fig. 2. Unit cells for three examples of two-dimensional photonic crystals.

tion symmetries with respect to the x and y axes. This implies that the dispersion relations have reflection symmetries with respect to the α and β axes on the plane of Bloch wave vector $\mathbf{k} = (\alpha, \beta)$. Therefore, the irreducible Brillouin zone is the rectangle bounded by the four points: $\Gamma = (0, 0)$, $X = (\pi/L_1, 0)$, $M = (\pi/L_1, \pi/L_2)$ and $X' = (0, \pi/L_2)$. Using $N_1 = 8$ and $N_2 = 10$ points on the short and long edges of the rectangular unit cell, respectively, and $m = 128$ points to discretize the boundary of ellipse, we obtain the band diagram shown in Fig. 3. The horizontal axis corresponds to the four edges and one diagonal of the irreducible Brillouin zone. The vertical axis is the normalized frequency $\omega L_2/(2\pi c)$. The dashed and the solid curves correspond to the E and H polarizations, respectively. To validate our results, we have repeated the calculations for $\omega L_1/(2\pi c) = 0.15$, 0.2, 0.4 and 0.5, using various values of N_1, N_2 and m. Consistent results are obtained for $N_1 \leqslant 14$, $N_2 \leqslant 18$ and $m \leqslant 512$. In [38], a complete bandgap (for both polarizations) was found for $r_1 = 0.38L_2$ and $r_2 = 0.45L_2$. We are able to confirm the existence of a complete bandgap. However, since the air-holes are very close to each other (the shortest distance between two air-holes is only $0.01L_2$), it is difficult to verify the accuracy of the solutions, especially for the H polarization.

The second example is a square lattice of elliptic dielectric rods in air, where the dielectric constant of the rods is $\epsilon_1 = n_1^2 = 14$. As shown in Fig. 2(b), the major axis of the elliptic rods and the x-axis form a 45° angle. The lengths of the semi-axes are $r_1 = 0.424L$ and $r_2 = 0.212L$. The structure has reflection symmetries with respect to straight lines $y = \pm x$. This implies that the dispersion relations (9) also have reflection symmetries with respect to the lines $\beta = \pm\alpha$ on the $\alpha\beta$ plane. Therefore, the irreducible Brillouin zone is the triangle with vertices at $\Gamma = (0, 0)$, $M = (\pi/L, \pi/L)$ and $M' = (-\pi/L, \pi/L)$. Using $N = 6$ sampling points on each edge of

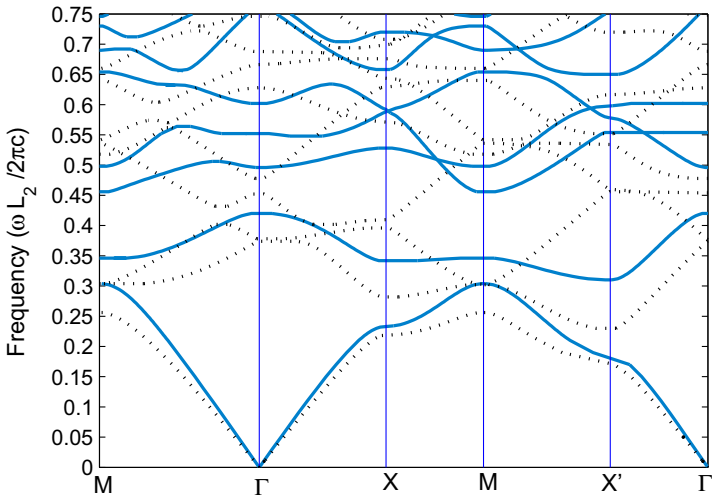

Fig. 3. Band structure of a rectangular lattice of elliptic air-holes in a dielectric medium ($\epsilon_2 = 11.4$). The solid and dashed lines represent the H and E polarizations, respectively.

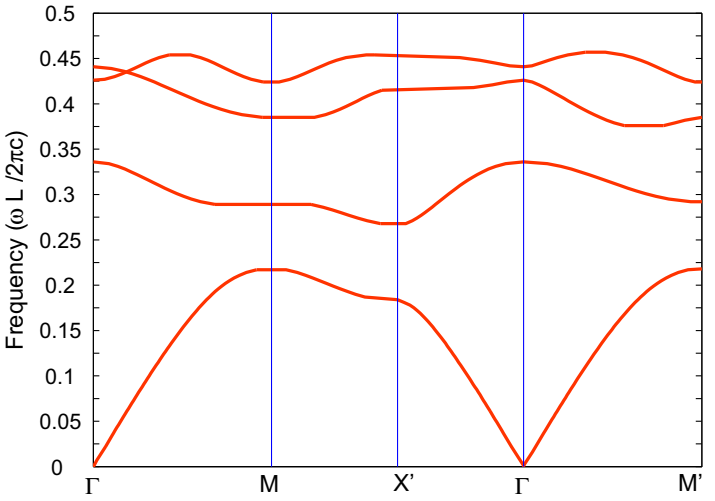

Fig. 4. Band structure for a square lattice of elliptic dielectric rods ($\epsilon_1 = 14$) in air (the E polarization).

the unit cell and $m = 128$ points to discretize the boundary of the ellipse, we obtain the dispersion curves for the E polarization as shown in Fig. 4. On the top edge $M'M$, the dispersion curves are symmetric with respect to the mid-point $X' = (0, \pi/L)$. In fact, Eq. (14) can be written as $\omega_k(\alpha, \pi/L) = \omega_k(-\alpha, \pi/L)$. Therefore, the band diagram shows only half of the top edge, from M to X', but it also includes a line from M' to Γ. Our results agree with those of Feng et al. [39] who used a plane wave expansion method. The results shown in Fig. 4 are verified with other values of N and m for a few frequencies.

Finally, we consider a square lattice of dielectric rods with a kite-shaped cross section as shown in Fig. 2(c). The dielectric constant of the rods is $\epsilon_1 = n_1^2 = 13$ and the background medium is air. The boundary of the rod in the square unit cell (given as $0 < x, y < L$) has the following parametric representation:

$$x = \frac{L}{6}(2.35 + \cos\theta + 0.65\cos 2\theta), \quad y = L(0.5 + 0.25\sin\theta)$$

for $0 \leqslant \theta \leqslant 2\pi$. Since the refractive index is real, we can apply (13) and consider only half of the first Brillouin zone with positive α. On the other hand, the structure has a reflection symmetry with respect to the x-axis. This

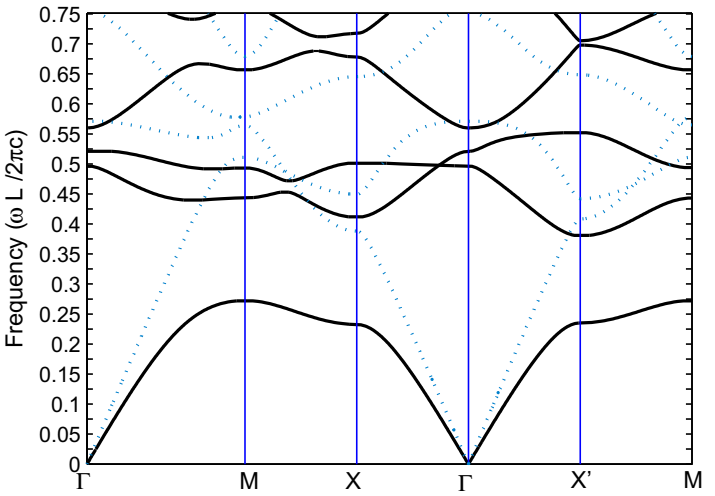

Fig. 5. Band structure for a square lattice of kite-shaped dielectric rods ($\epsilon_1 = 13$) in air. The solid and dashed lines represent the E and H polarizations, respectively.

Table 1
Computed Bloch wave vector component for $\omega L/(2\pi c) = 0.4$

N	$\mathbf{k}$ on $\Gamma X'$	$\mathbf{k}$ on $X'M$
5	0.58314	0.30949
6	0.58086	0.31273
7	0.58106	0.31260
8	0.58148	0.31189
9	0.58176	0.31147
10	0.58152	0.31186
11	0.58176	0.31166
12	0.58160	0.31166
13	0.58168	0.31171
14	0.58168	0.31168

implies that the dispersion relations satisfy $\omega_k(\alpha,\beta) = \omega(\alpha,-\beta)$. Therefore, the irreducible Brillouin zone is the square with corners at $\Gamma = (0,0)$, $X = (\pi/L, 0)$, $M = (\pi/L, \pi/L)$ and $X' = (0, \pi/L)$. Using $N = 7$ points on each edge of the unit cell and $m = 128$ on the boundary of the kite-shaped rod, we obtain the dispersion curves shown in Fig. 5. These results are verified with repeated calculations using other values of N and m for $\omega L/(2\pi c) = 0.07$, 0.25 and 0.4. The case for $\omega L/(2\pi c) = 0.4$ and $m = 128$ is given in Table 1. It seems that 3 or 4 significant digits can be obtained with $N \leqslant 10$. Since the global expansion (32) is used to construct the DtN map, ill-conditioning will affect the accuracy when N is too large.

In the above calculations, we solved the eigenvalue problems 24, 29, 30 and 31 for ρ (i.e., ρ_1 or ρ_2) on the unit circle. In practice, this condition is replaced by $|1 - |\rho|| \leqslant \delta$, where δ is on the order of 10^{-3}. Our method is efficient, since the size of the matrices is very small.

5. Conclusions

For 2D PhCs containing cylinders with arbitrary cross sections, we developed a boundary integral equation method for constructing the DtN maps of the unit cells and applied the DtN maps to compute the band structures. Numerical examples include dielectric rods in air and air-holes in dielectric media, where the rods and air-holes have elliptic or kite-shaped cross sections. The DtN map is obtained by approximating the general wave field inside a unit cell by a sum of J special solutions and evaluating the field and its normal derivative at J sampling points on the boundary of the unit cell. The special solutions are obtained from solving scattering problems for a single cylinder on the entire plane. The boundary integral equation method is ideal for the scattering problem, since the refractive index is constant inside and outside the cylinder. The different special solutions are related to the scattering of different plane incident waves on the same cylinder, and they can be solved together efficiently, since they correspond to linear systems with the same coefficient matrix and different right hand sides. The required number of operations for constructing the DtN map is $O(m^3)$, where m is the number of points for discretizing the boundary of the cylinder. The band structures are calculated from linear eigenvalue problems of small matrices. The sizes of these matrices are $J \times J$ or less. In the numerical examples, reasonably accurate solutions have been obtained with $m = 128$ and $J = 24$, 28 and 36.

The DtN maps of a unit cell has also been used to develop efficient numerical methods for analyzing the transmission and reflection of finite PhCs [35,36].

References

[1] E. Yablonovitch, Inhibited spontaneous emission in solid-state physics and electronics, Phys. Rev. Lett. 58 (1987) 2059–2062.
[2] S. John, Strong localization of photons in certain disordered dielectric superlattices, Phys. Rev. Lett. 58 (1987) 2486–2489.
[3] J.D. Joannopoulos, R.D. Meade, J.N. Winn, Photonic Crystals: Molding the Flow of Light, Princeton University Press, Princeton, NJ, 1995.
[4] O. Toader, S. John, Photonic band gap enhancement in frequency-dependent dielectrics, Phys. Rev. E 70 (2004). Art. No. 046605.
[5] M. Qiu, S.L. He, A nonorthogonal finite-difference time-domain method for computing the band structure of a two-dimensional photonic crystal with dielectric and metallic inclusions, J. Appl. Phys. 87 (12) (2000) 8268–8275.

[6] S.L. He, S.S. Xiao, L.F. Shen, J.P. He, J. Fu, A new finite-difference time-domain method for photonic crystals consisting of nearly-free-electron metals, J. Phys. A – Math. General 34 (45) (2001) 9713–9721.
[7] K.M. Leung, Y.F. Liu, Full vector wave calculation of photonic band structures in face-centered-cubic dielectric media, Phys. Rev. Lett. 65 (1990) 2646–2649.
[8] Z. Zhang, S. Satpathy, Electromagnetic wave propagation in periodic structures – Bloch wave solution of Maxwell's equations, Phys. Rev. Lett. 65 (1990) 2650–2653.
[9] K.M. Ho, C.T. Chan, C.M. Soukoulis, Existence of a photonic gap in periodic dielectric structures, Phys. Rev. Lett. 65 (1990) 3152–3155.
[10] R.D. Meade, A.M. Rappe, K.D. Brommer, J.D. Joannopoulos, O.L. Alerhand, Accurate theoretical analysis of photonic band-gap materials, Phys. Rev. B 48 (1993) 8434–8437.
[11] S.G. Johnson, J.D. Joannopoulos, Block-iterative frequency-domain methods for Maxwell's equations in a planewave basis, Opt. Express 8 (2001) 173–190.
[12] A. Figotin, Y.A. Godin, The computation of spectra of some 2D photonic crystals, J. Comput. Phys. 136 (1997) 585–598.
[13] X. Checoury, J.M. Lourtioz, Wavelet method for computing band diagrams of 2D photonic crystals, Opt. Commun. 259 (2006) 360–365.
[14] D.C. Dobson, An efficient method for band structure calculations in 2D photonic crystals, J. Comput. Phys. 149 (1999) 363–379.
[15] W. Axmann, P. Kuchment, An efficient finite element method for computing spectra of photonic and acoustic band-gap materials: I. Scalar case, J. Comput. Phys. 150 (1999) 468–481.
[16] M.C. Lin, R.F. Jao, Finite element analysis of photon density of states for two-dimensional photonic crystals with in-plane light propagation, Opt. Express 15 (2007) 207–218.
[17] H.Y.D. Yang, Finite difference analysis of 2-D photonic crystals, IEEE Trans. Microwave Theory Tech. 44 (1996) 2688–2695.
[18] L.F. Shen, S.L. He, S.S. Xiao, A finite-difference eigenvalue algorithm for calculating the band structure of a photonic crystal, Comput. Phys. Commun. 143 (2002) 213–221.
[19] C.P. Yu, H.C. Chang, Applications of the finite difference mode solution method to photonic crystal structures, Opt. Quantum Electron. 36 (2004) 145–163.
[20] S. Guo, F. Wu, S. Albin, R.S. Rogowski, Photonic band gap analysis using finite-difference frequency-domain method, Opt. Express 12 (2004) 1741–1746.
[21] P.J. Chiang, C.P. Yu, H.C. Chang, Analysis of two-dimensional photonic crystals using a multidomain pseudospectral method, Phys. Rev. E 75 (2007). Art. No. 026703.
[22] M. Marrone, V.F. Rodriguez-Esquerre, H.E. Hernández-Figueroa, Novel numerical method for the analysis of 2D photonic crystals: the cell method, Opt. Express 10 (2002) 1299–1304.
[23] S. Jun, Y.S. Cho, S. Im, Moving least-square method for the band-structure calculation of 2D photonic crystals, Opt. Express 11 (2003) 541–551.
[24] E. Moreno, D. Erni, C. Hafner, Band structure computations of metallic photonic crystals with the multiple multipole method, Phys. Rev. B 65 (2002). Art. No. 155120.
[25] S.Y. Shi, C.H. Chen, D.W. Prather, Revised plane wave method for dispersive material and its application to band structure calculations of photonic crystal slabs, Appl. Phys. Lett. 86 (2005). Art. No. 043104.
[26] J.B. Pendry, A. MacKinnon, Calculation of photon dispersion relations, Phys. Rev. Lett. 69 (1992) 2772–2775.
[27] J.B. Pendry, Calculating photonic band structure, J. Phys. Condensed Matter 8 (1996) 1085–1108.
[28] L.C. Botten, N.A. Nicorovici, R.C. McPhedran, et al., Photonic band structure calculations using scattering matrices, Phys. Rev. E 64 (2001) 046603.
[29] J. Yuan, Y.Y. Lu, Photonic bandgap calculations using Dirichlet-to-Neumann maps, J. Opt. Soc. Am. 23 (2006) 3217–3222.
[30] J. Yuan, Y.Y. Lu, Computing photonic band structures by Dirichlet-to-Neumann maps: the triangular lattice, Opt. Commun. 273 (2007) 114–120.
[31] P. Lalanne, G.M. Morris, Highly improved convergence of the coupled-wave method for TM polarization, J. Opt. Soc. Am. 13 (1996) 779–784.
[32] L. Li, Formulation and comparison of two recursive matrix algorithms for modeling layered diffraction gratings, J. Opt. Soc. Am. 13 (1996) 1024–1035.
[33] G. Bao, Z.M. Chen, H.J. Wu, Adaptive finite-element method for diffraction gratings, J. Opt. Soc. Am. 22 (2005) 1106–1114.
[34] K. Dossou, M.A. Byrne, L.C. Botten, Finite element computation of grating scattering matrices and application to photonic crystal band calculations, J. Comput. Phys. 219 (2006) 120–143.
[35] Y. Huang, Y.Y. Lu, Scattering from periodic arrays of cylinders by Dirichlet-to-Neumann maps, J. Lightwave Technol. 24 (2006) 3448–3453.
[36] Y. Huang, Y.Y. Lu, Modeling photonic crystals with complex unit cells by Dirichlet-to-Neumann maps, J. Comput. Math. 25 (2007) 337–349.
[37] D. Colton, R. Kress, Inverse Acoustic and Electromagnetic Scattering Theory, second ed., Springer-Verlag, Berlin, 1998.
[38] M. Qiu, S. He, Large complete band gap in two-dimensional photonic crystals with elliptic air holes, Phys. Rev. B 60 (1999) 10610–10612.
[39] S. Feng, Z.Y. Li, Z.F. Feng, et al., Imaging properties of an elliptical-rod photonic-crystal slab lens, Phys. Rev. B 72 (2005) 075101.
[40] J.M. Harrison, P. Kuchment, A. Sobolev, B. Winn, On occurrence of spectral edges for periodic operators inside the Brillouin zone, J. Phys. A: Math. Theor. 40 (2007) 7597–7618.